Spectrochimica Acta Part A: Molecular and Biomolecular Spectroscopy 270 (2022) 120846

Contents lists available at ScienceDirect

Spectrochimica Acta Part A: Molecular and Biomolecular Spectroscopy

journal homepage: www.elsevier.com/locate/saa

Water binding to the atmospheric oxidation product methyl vinyl ketone

Carlos Cabezas [a,*], Marcos Juanes [b], Rizalina T. Saragi [b], Alberto Lesarri [c], Isabel Peña [b,*]

[a] Instituto de Física Fundamental (IFF–CSIC), Group of Molecular Astrophysics, C/ Serrano 121, Madrid 28006, Spain
[b] Departamento de Química Física y Química Inorgánica, Facultad de Ciencias, Universidad de Valladolid, Paseo de Belén 7, Valladolid 47011, Spain
[c] Departamento de Química Física y Química Inorgánica, Facultad de Ciencias–I.U. CINQUIMA, Universidad de Valladolid, Paseo de Belén 7, Valladolid 47011, Spain

HIGHLIGHTS

- Four 1:1 complexes of methyl vinyl ketone – water identified.
- Preference of water for an antiperiplanar conformation of methyl vinyl ketone.
- Primary O – H···O and secondary C – H···O hydrogen bond interactions.
- Threefold methyl internal rotation barrier heights determined.

GRAPHICAL ABSTRACT

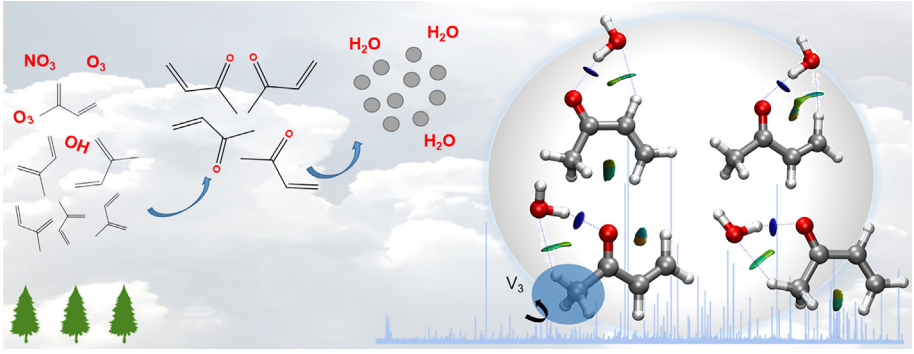

ARTICLE INFO

Article history:
Received 20 October 2021
Accepted 29 December 2021
Available online 7 January 2022

ABSTRACT

Methyl vinyl ketone is one of the major oxidation products of isoprene, and therefore, an important precursor of secondary organic aerosol. Understanding its interactions with water is relevant to gain insight into aerosol formation and improve the predictive power of atmospheric chemistry models. The molecular complex formed between methyl vinyl ketone and water has been generated in a supersonic jet and characterized using high-resolution microwave spectroscopy in combination with quantum chemistry calculations. In this study, we show that methyl vinyl ketone interacts with water forming four 1:1 isomers connected by O – H···O and C – H···O hydrogen bond interactions. Water has been found to preferentially bind to the antiperiplanar conformation of methyl vinyl ketone. Evidence of a large amplitude motion arising from the methyl internal rotation has been found in the rotational spectra of the dimer. The threefold methyl internal rotation barrier heights have been further determined and discussed for all the species.

1. Introduction

Secondary organic aerosol (SOA) constitutes a significant source of uncertainty in understanding air pollution and has a profound impact on the radiation balance and human health [1]. In the atmosphere, oxidation of volatile organic compounds (VOCs) produces low – volatility oxygenated products, which have a major influence on SOA formation [2], by condensing onto preexisting particles or participating in nucleation [3]. Although significant advances have been made in the identification of SOA precursors, information on the mechanisms for the photochemical gas – to – particle conversion of VOCs or how molecules interact with each other to form clusters is yet to be revealed.

The growing interest in biogenically emitted volatile organic compounds (BVOCs) produced by plants, mainly isoprene and terpenes, has prompted investigations of the SOA forming potential of these compounds [3], which may play an important role in atmospheric chemistry. Isoprene (2 – methyl – 1,3 – butadiene, C_5H_8) is a highly abundant species in the atmosphere and reacts

* Corresponding authors.
E-mail addresses: carlos.cabezas@csic.es (C. Cabezas), ipencal@qf.uva.es (I. Peña).

https://doi.org/10.1016/j.saa.2021.120846
1386-1425/

primarily with OH radicals during the day and with O_3 and NO_3 radicals during the night [4,5]. Methyl vinyl ketone (MVK, C_4H_6O), like methacrolein, is a major oxidation product of isoprene and contributes actively to the creation of tropospheric ozone [6] and SOA [7]. Studies carried out in atmospheric simulation chambers or from atmospheric sampling or modelling have shown that oxidation of hydrocarbons released by plants leads to semi – volatile organic compounds, which can be absorbed and partitioned into the condensed phase to form SOA. Nevertheless, SOA formation at molecular level is not well understood, specifically, the role water may play in nucleation and oxidation processes [8].

Water is ubiquitous in the troposphere, and therefore, has influence on the evolution of oxidation products changing the composition and physical properties of SOA [9,10]. It has been reported that an increase in relative humidity leads to an increment in SOA yields due to water absorption in the aerosol phase, which favors the condensation of semi – volatile compounds [11,12]. Additionally, some studies have shown that water can alter reaction barriers heights upon complexation, showing a catalytic or inhibitory effect with significant consequences for atmospheric reactions [13]. A recent study demonstrates that SOA formation from isoprene ozonolysis is inhibited by the addition of water vapor [14]. Elucidation of the intermolecular interactions between oxidation products such as MVK and water is an essential step to understand the effect water has on the mechanism of SOA formation.

Jet – cooled Fourier transform microwave (FTMW) spectroscopy constitutes an ideal technique for the study of molecular clusters since it provides accurate structural information in the gas phase, being able to distinguish between slightly different configurations of complexes without ambiguity [15]. It has been applied to the investigation of a few hydrates formed by products of monoterpene atmospheric oxidation [16–21]. However, to our knowledge, there are no studies addressing water binding to the highly abundant products of isoprene atmospheric oxidation. Here, we present an investigation of the interactions of MVK with water using high-resolution microwave spectroscopy in combination with quantum chemical calculations in order to broaden the structural information on the hydrates of oxidation products and improve our understanding of SOA formation.

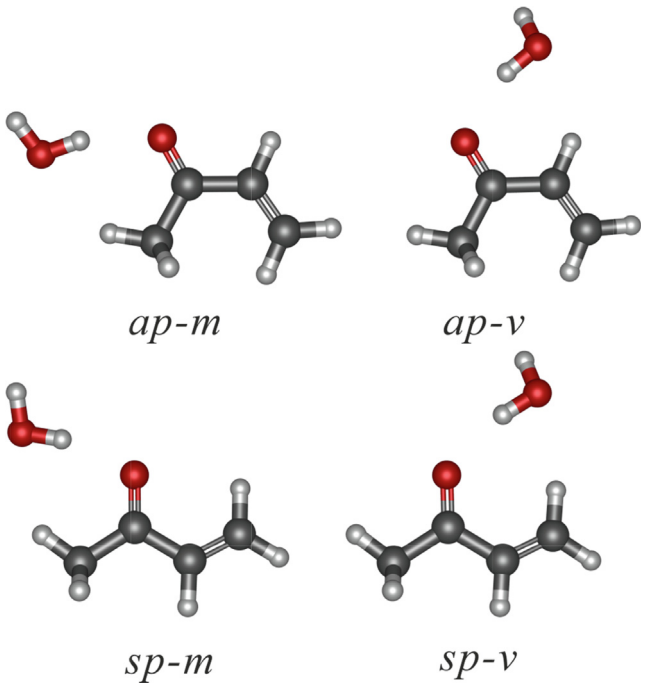

Fig. 1. Molecular structures for the four MVK – H_2O isomers calculated at the MP2/6–311++G(d,p) level of theory.

MVK presents two stable conformations, antiperiplanar (*ap*) and synperiplanar (*sp*), showing a *trans* and *cis* arrangement of the two double bonds, respectively (Fig. 1). The rotational spectrum of MVK was first characterized by Foster et al. in 1965 with the detection of the most stable *ap* conformer [22]. The analysis of the *A–E* doublets arising from the internal rotation of the methyl group allowed the determination of the value of the internal rotation barrier. The rotational spectrum of MVK was later reinvestigated using a molecular beam Fourier transform microwave spectrometer [23]. The less stable *sp* conformer was detected for the first time, and the methyl barrier heights of the *ap* and *sp* species were also determined. More recently, quantum chemical calculations coupled to high – resolution millimetre-wave spectroscopy have been performed to characterize the ground and first excited vibrational states of the two most stable conformers [24]. In the present work, we aim to generate and characterize for the first time the 1:1 MVK–H_2O adducts and reveal its hydrogen – bond (HB) topology. We will try to answer some intriguing questions: will hydrogen bonding help stabilize *sp* versus *ap* MVK? How will complexation and hydrogen bonding interactions affect potential large amplitude motions such as the methyl internal rotation?

2. Quantum chemical calculations

Quantum chemical calculations were carried out to examine the potential energy surface of the MVK–H_2O molecular system. Geometry optimizations for all the plausible adducts formed by each of the MVK isomers and a water molecule were done using the Møller – Plesset (MP2) [25] perturbation theory in the frozen core approximation method combined with the Pople triple – ζ basis set (6–311++G(d,p)) [26]. All the calculations were carried out using the Gaussian 16 program package [27].

As it can be seen in Fig. 1, the water molecule can link to MVK in two different positions corresponding to the non – equivalent lone pairs of the oxygen atom, which produces a total of four isomers. For the isomers formed by the *ap* species, the water molecule forms two HBs with the MVK molecule. One of the HBs is formed between one of the water H atoms and the oxygen of the MVK molecule. The second HB is established between the oxygen atom of the water molecule and one H atom of the methyl (*m*) group or the H atom of the – CH group of the vinyl (*v*) moiety. Hence, the *ap* – *m* isomer displays the HB between water O and the H atom of the methyl group, while in the *ap* – *v* water, oxygen links to the vinyl moiety. For the isomers derived from *sp* isomer, there exist two possibilities as well. In the *sp* – *m* species, the water links with MVK through the carbonyl group and one H of the methyl group, while in the *sp* – *v* isomer, the water interacts with the carbonyl group and the $-CH_2$ group of the vinyl moiety.

The rotational constants and the electric dipole moment components predicted from our calculations for the four MVK–H_2O isomers are shown in Table 1. The relative energies, ZPE and Gibbs energies for the four species are also given in Table 1.

3. Experimental

The rotational spectra for the MVK–H_2O isomers were recorded using two different experimental setups. The first experiments were carried out using the broadband microwave spectrometer at the University of Valladolid, described elsewhere [28], to collect swiftly the rotational spectra of the species present in the gas–phase mixture. The MVK (stated purity ≥ 99%) sample was pur-

Table 1
Theoretical rotational constants, electric dipole moment components and relative energies for the four predicted MVK – H_2O isomers calculated at the MP2/6–311++G(d,p) level of theory.

	ap – *m*	*ap* – *v*	*sp* – *m*	*sp* – *v*
A /MHz	8619	4362	6694	4659
B /MHz	1446	1992	1566	1930
C /MHz	1251	1382	1285	1379
$\|\mu_a\|$/D	3.1	2.9	2.9	2.9
$\|\mu_b\|$/D	0.3	0.2	0.6	0.5
$\|\mu_c\|$/D	0.6	0.8	0.6	0.7
E^a/h	−306.9166405	−306.9170073	−306.9159442	−306.9161053
ΔE^b/cm^{-1}	81	0	233	198
$\Delta(E + ZPE)^c$/cm^{-1}	33	0	146	150
ΔG^d/cm^{-1}	0	63	43	113
E_B^e/kcal mol^{-1}	−3.66	−3.78	−3.68	−3.73
E_B^f/kcal mol^{-1}	−2.69	−2.75	−2.67	−2.66

[a] Absolute energies.
[b] Relative energy to that of *ap* – *v* isomer.
[c] Zero – point corrected energy relative to that of *ap* – *v* isomer.
[d] Relative Gibbs free energy to that of *ap* – *m* isomer.
[e] Binding energy for the complex relative to that of separated *ap* – MVK or *sp* – MVK and H_2O molecules (no BSSE correction).
[f] ZPE corrected binding energy, which is the energy difference between the dimer and its subunits (no BSSE correction).

chased from Sigma Aldrich and was used without further purification. MVK and water samples were placed in two separated reservoirs at room temperature inserted in the gas line outside of the vacuum chamber. The carrier gas neon was allowed to flow over the MVK and water reservoirs at backing pressures of 3 bar, expanding through a pulsed nozzle (0.8 mm diameter, Parker General Valve, Series 9). For each gas pulse, the molecules were polarized with a series of 5 microwave chirps of 4 μs duration spanning 2 to 8 GHz. The chirped pulse was generated with an arbitrary waveform generator (Tektronix AWG 70002A), amplified to 20 W with a solid-state MW amplifier and broadcasted perpendicularly to the propagation of the jet expansion through a horn antenna. A molecular transient emission spanning 40 μs is then detected through a second horn and amplified by a low noise MW amplifier. A total of 600 k free-induction decays (FIDs) were co – added in a digital oscilloscope and Fourier transformed with a Kaiser – Bessel window function to give the broadband rotational spectrum in the frequency domain. All the frequencies are referenced to a 10 MHz Rb standard. The accuracy of the frequency measurements was better than 10 kHz.

Further experiments were carried out using the ^{18}O and deuterated isotopic species of water, namely $H_2^{18}O$, D_2O, DOH and HOD. Commercial samples of $H_2^{18}O$ (stated purity ≥ 99%) and D_2O (stated purity ≥ 99%) were used to observe the spectra of MVK – $H_2^{18}O$ and MVK – D_2O. MVK – DOH and MVK – HOD complexes were produced by filling the liquid container with a 1:1 mixture of D_2O and H_2O.

A cavity – based [29] Fourier transform microwave spectrometer [30] with coaxial injection and sub – Doppler resolution were carried out to cover the 8–16 GHz frequency range [31]. MVK and water samples were placed in two separated reservoirs in the carrier gas line outside of the vacuum chamber. Neon at a stagnation pressure of 3 bar was passed over the liquid reservoirs at room temperature and expanded through a solenoid valve (Parker, Series 9, nozzle diameter 0.5 mm) into the Fabry – Pérot cavity. The spectral line positions were determined after Fourier transformation of the time – domain FID signal with 8 k data points, recorded with 100 ns sample intervals. Each rotational transition appears as a doublet due to the Doppler effect. The resonance frequencies were calculated as the arithmetic mean of the frequencies of the Doppler components. The estimated accuracy of the frequency measurements was better than 3 kHz. Lines separated by>7 kHz were resolvable.

4. Results and discussion

4.1. Rotational spectra: Analysis and conformational identification

The 2–8 GHz broadband rotational spectrum recorded for MVK – H_2O isomers is shown in Fig. 2. Once the most intense lines from the two observed conformers of MVK [24] were removed from the spectrum, identification of spectral patterns belonging to four different species was accomplished. The four species showed only *a* – type rotational spectrum and their rotational transitions appeared very close to the predicted frequencies. *b* – and *c* – type rotational spectra could not be observed probably due to the low intensity of the signals and the low predicted values of the corresponding dipole moment components. As can be seen in Fig. 2(a), most of the lines are split into two symmetry components, *A* and *E*, as a result of the interaction between the C_3-methyl group internal rotation and the overall rotation. However, in some transitions, the *A* and *E* components are not resolved, as shown in Fig. 2(b). At this point we took advantage of the higher resolution of the cavity – based spectrometer to fully resolve the internal rotation doublets (Fig. 2(c)). A total of 26, 24, 24 and 22 *A* and *E* components were measured for the *ap* – *m*, *ap* – *v*, *sp* – *m* and *sp* – *v* isomers, respectively (see Tables S1 – S4 from Supplementary Information). All the observed rotational frequencies for *A* and *E* components were included in a least – squares fit using the XIAM program [32], which is based on the Watson's *A* – reduced Hamiltonian [33] supplemented with the internal rotation combined axis method in the form given by Woods [34]. The semirigid rotor analysis rendered the experimental rotational constants listed in Table 2.

A definite identification of the isomers was achieved from the observation of the spectra of the substituted isotopologues. First, we replaced H_2O by $H_2^{18}O$ and recorded the rotational spectra for MVK – $H_2^{18}O$ complexes. We measured 14, 8, 11 and 6 *A* and *E* components for the *ap* – *m*, *ap* – *v*, *sp* – *m* and *sp* – *v* isomers in the 2–8 GHz region, respectively, which were similarly fitted using the XIAM program. Only the values for *B* and *C* rotational constants were floated in the fit due to the low number of observed lines for MVK – $H_2^{18}O$ complexes. The rotational constant *A* was fixed to the scaled *ab initio* value, while the internal rotation spectroscopic parameters (V_3, F_0, δ and ε) were fixed to those for the MVK – H_2O parent species. The results from these fits are shown in Table 3. Then, we used D_2O to observe the MVK – D_2O complexes and a 1:1 mixture of H_2O and D_2O to observe the

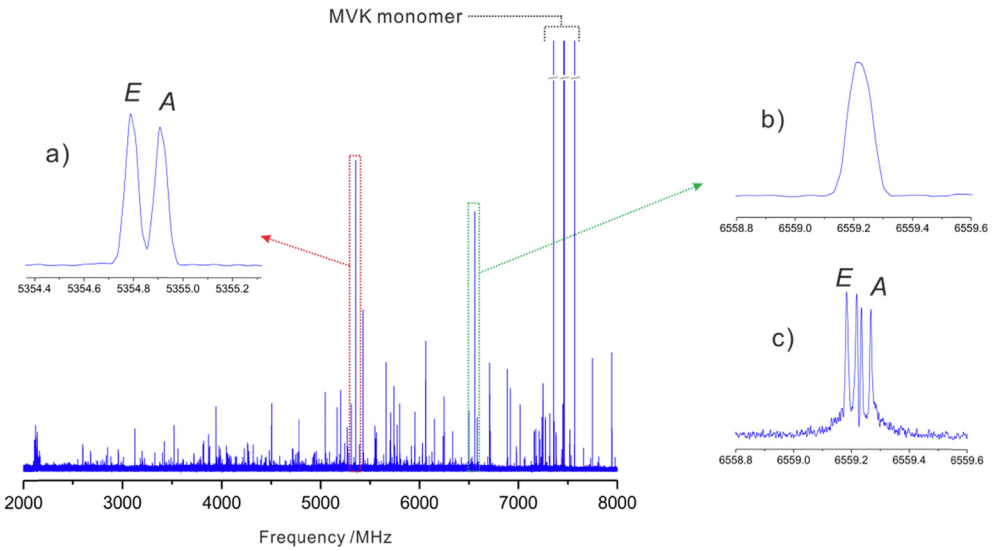

Fig. 2. Broadband rotational spectrum of MVK – H_2O in the 2–8 GHz frequency region. (a) Detail of the $2_{0,2} \leftarrow 1_{0,1}$ rotational transition of the *ap* – *m* isomer with the *A* – *E* internal rotation components clearly differentiated. (b) Detail of the $2_{0,2} \leftarrow 1_{0,1}$ rotational transition of the *ap* – *v* isomer with the unresolved *A* – *E* internal rotation components. (c) $2_{0,2} \leftarrow 1_{0,1}$ rotational transition of the *ap* – *v* isomer observed with the higher resolution of the cavity – based FTMW spectrometer. It is split into four lines due to internal rotation (*A* – *E* doublet) and Doppler effects.

Table 2
Experimental rotational constants for the four MVK – H_2O isomers observed in this work.

	ap – *m*	*ap* – *v*	*sp* – *m*	*sp* – *v*
A /MHz	8711.95(27)[a]	4383.567(17)	6766.47(19)	4605.497(24)
B /MHz	1435.30513(87)	1960.4041(16)	1557.64951(82)	1920.4197(14)
C /MHz	1243.98409(81)	1367.3002(11)	1278.08010(74)	1368.73780(91)
Δ_J /kHz	0.6436(73)	1.598(21)	0.568(10)	0.799(24)
Δ_{JK} /kHz	–	–	5.92(47)	7.17(70)
δ_J /kHz	0.0809(93)	0.545(19)	0.0560(81)	0.232(16)
V_3^b/cm^{-1}	389.80(43)	418.5(17)	349.59(26)	359.99(34)
F_0^c/GHz	157.882[d]	158.974[d]	156.367[d]	157.194[d]
δ^e/rad	1.7984(49)	0.503(14)	1.0926(18)	2.6943(52)
ε^f/rad	0.021[d]	0.099[d]	0.207(17)	0.023[d]
N^g	26	24	24	22
σ^h/kHz	3.3	4.9	3.0	4.0

[a] Values in parentheses denote 1σ errors, applied to the last digit. [b] Barrier height of the threefold methyl internal rotation. [c] Rotational constant of the methyl top. [d] Fixed to the *ab initio* value. [e] Angle between the principal axis of the molecule and the internal rotation axis. [f] Angle between the principal axis of the molecule and the projection of the internal rotation axis onto *xy* – plane. [g] Number of *A*/*E* components included in the fit. [h] rms error of the fit.

MVK – DOH and MVK – HOD complexes. MVK – DOH refers to the situation where the bonded H atom of the water subunit is replaced by a D atom, while MVK – HOD refers to the case where the non-bonded H atom of water is replaced by a D atom. The spectra for deuterated species were much weaker than that obtained for MVK – $H_2^{18}O$, and thus, only the spectra for the *ap* – *m* species could be detected for the MVK – D_2O, MVK – DOH and MVK – HOD isotopic species. The analysis of the rotational transitions for this isomer was done in the same manner as those for the MVK – $H_2^{18}O$, and only the *B* and *C* rotational constants could be experimentally determined. Results are shown in Table 4. All the observed frequencies are listed in the Supplementary Information (Tables S5 and S6).

The conformational identification of the four MVK – H_2O isomers was achieved by comparing the experimental and theoretical values of the rotational constants, shown in Tables 1 and 2. Due to the very good agreement found between them, with relative deviations between 0.5 and 1.6 %, the assignments can be considered unambiguous. Further confirmation was achieved from the obser-

Table 3
Experimental rotational constants for the four MVK – $H_2^{18}O$ complexes.[a]

	ap – *m*	*ap* – *v*	*sp* – *m*	*sp* – *v*
A /MHz	8703.69[b]	4376.97[b]	6735.03[b]	4584.64[b]
B /MHz	1357.5853(16)[c]	1840.8971(48)	1471.7482(26)	1807.955(22)
C /MHz	1185.1029(16)	1307.4496(44)	1218.7710(19)	1308.997(20)
N [d]	14	8	11	6
σ [e]/kHz	10.6	17.3	10.2	18.2

[a] Centrifugal distortion constants were kept fixed to those found for the parent species, which are shown in Table 2. [b] Derived value from the fit keeping B_J parameter fixed (see text). [c] Values in parentheses denote 1σ errors, applied to the last digit. [d] Number of *A*/*E* components included in the fit. [e] rms error of the fit.

Table 4
Experimental rotational constants for the deuterated isotopologues of the *ap* – *m* isomer.[a]

	MVK···D_2O	MVK···DOH	MVK···HOD
A /MHz	8661.15[b]	8689.01[b]	8682.40[b]
B /MHz	1359.0031(21)[c]	1414.3360(23)	1377.7437(21)
C /MHz	1185.3999(22)	1227.7012(18)	1200.0788(20)
N [d]	12	12	10
σ [e]/kHz	13.5	9.8	11.3

[a] Centrifugal distortion constants were kept fixed to those found for the parent species, which are shown in Table 2. [b] Derived value from the fit keeping B_J parameter fixed in the fit (see text). [c] Values in parentheses denote 1σ errors, applied to the last digit. [d] Number of *A*/*E* components included in the fit. [e] rms error of the fit.

vation of their $H_2^{18}O$, DOH, HOD and D_2O isotopologues (Tables 3 and 4).

The relative abundances of the observed MVK – H_2O isomers were estimated by measuring the intensities of a set of three common *a* – type transitions in the broadband spectrum, which were normalized by the square of the *a* – component dipole moment. The relative abundances were found to be *ap* – *v* > *ap* – *m* > *sp* – *m* > *sp* – *v* = 1 > 0.6 > 0.3 > 0.1, in agreement with the zero – point corrected binding energies predicted at the MP2/6–311++G(d,p) level of theory (Table 1). This result is not in total agreement with the relative Gibbs energies of the monohydrates. However, the values above can be affected by collisional relaxation from higher-energy species in the supersonic jet. The most abundant isomers adopt the *ap* conformation, which is also the most abundant one for bare MVK in the gas phase [24]. Hence, the MVK – H_2O isomers follow the same abundance trend as the MVK monomers, and thus, it seems that HBs between MVK and water do not help stabilize *sp* – MVK versus *ap* – MVK.

4.2. Intermolecular interactions

The binding interactions have been visualized using the NCI method [35], based on the electron density and its derivatives. The strength of the intermolecular interactions is estimated through the contributions to the Laplacian of the density along the axes of maximal variation. The NCI plots of Fig. 3 shows blue isosurfaces indicating attractive O – H···O HBs and green isosurfaces for the weaker attractive C – H···O and dispersion interactions. Primary O – H···O HBs lengths are predicted to have the same value (1.94 Å) in the four isomers and are similar to those predicted for other hydrates containing a ketone [21]. However, significant differences can be found in the theoretical values of C – H···O secondary interactions. The C – H···O hydrogen bonds in *ap* – *v* and *sp* – *v* (2.45 Å and 2.35 Å) are shorter and thus stronger than those in *ap* – *m* and *sp* – *m* (2.51 Å and 2.53 Å), which may play a stabilizing role in the emergence of *ap*-*v* as the global minimum at MP2 level of theory. The presence of secondary interactions can also be inferred from the non – linearity of the primary O – H···O HB, with predicted values of 162.5°, 160.4°, 164.0° and 164.9° for the isomers *ap* – *m*, *ap* – *v*, *sp* – *m* and *sp* – *v*, respectively. The non – observation of splittings due to tunnelling motions of the hydrogen atoms of water suggests that water molecules are firmly anchored to MVK. Similar behaviour has also been reported in previous studies of other H – bonded water containing complexes [17,36].

4.3. Structural information

The derived rotational constants of the isotopic species were used to determine the substitution coordinates of the oxygen and hydrogen atoms of the water subunit (Tables 5 and 6). These calculations were done using the Kraitchman's method [37] and the KRA program [38]. The substitution coordinates for the oxygen atom of the water subunit (Table 5) are in good agreement with those predicted *ab initio* for the four isomers. However, there are larger discrepancies for the derived values of the hydrogen atoms of the water subunit (Table 6). These differences can be attributed to the large change of mass on the D substitution and to the methyl top internal rotation which induces a vibrational motion in the water molecule altering the relative positions of the hydrogen atoms.

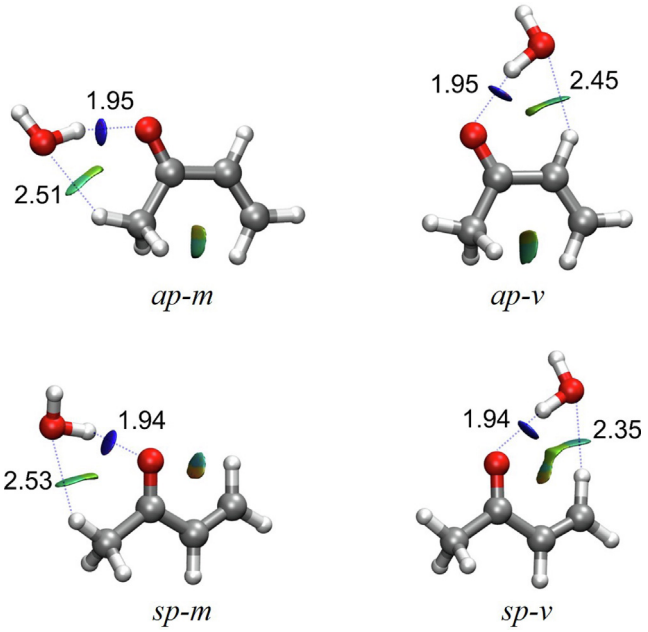

Fig. 3. Overlays of the MP2/6–311++G(d,p) structures of the observed isomers showing their NCI isosurfaces (*s* = 0.5). Intermolecular HBs are indicated with dashed lines and the bond lengths are given in Å.

A partial r_0 structure was derived for the HB parameters of the *ap* – *m* complex through a least-squares fit [38] using the experimental moments of inertia of the three isotopologues MVK – H_2O, MVK – $H_2^{18}O$ and MVK – D_2O. Since the *A* rotational constant could not be well determined, the best results were found when only *B* and *C* experimental rotational constants were used in the fit. Two distances and two angles of the intermolecular HBs O – H···O and C – H···O between MVK and water moieties could be determined while all other parameters were kept fixed to the MP2 theoretical values. The derived structural parameters are shown in Table 7. There is a good agreement in the distance and the angle defining the primary OH···O HB with a deviation less than 1% from the MP2/6–311++G(d,p) structure. Nevertheless, the fit rendered a higher value of the dihedral angle H – O – H···O compared with that predicted, probably due to the vibrational motions of the water molecule, which alter the position of the non-bonded hydrogen atom. For the C – H···O HB, a distance of 2.44 Å was obtained, which means a slightly stronger interaction than that predicted (2.51 Å). However, these results have to be taken with caution due to the plausible Ubbelohde effect.

4.4. Internal rotation

The analysis of the internal rotation splittings for the four MVK – H_2O complexes allowed us to determine the threefold methyl internal rotation barrier height (V_3) for all the species. Other structural parameters, related to the molecular axes and the internal rotation axis of the methyl top, denoted as δ and ε,

Table 5
Comparison between substitution and equilibrium MP2/6–311++G(d,p) coordinates determined for the oxygen atom of the water subunit in the four MVK – H_2O isomers.

	ap – *m*		*ap* – *v*		*sp* – *m*		*sp* – *v*	
	r_s	r_e	r_s	r_e	r_s	r_e	r_s	r_e
|*a*|[a]	3.20584(47)[b]	3.196	2.90870(52)	2.900	3.10470(49)	3.095	2.88479(60)	2.866
|*b*|	0.150(10)	0.141	0.3196(48)	0.310	0.4236(36)	0.422	0.5261(34)	0.517
|*c*|	0.087(18)	0.102	0[c]	0.063	0.109(14)	0.123	0.070(25)	0.056

[a] *a*, *b* and *c* are the coordinates in angstroms in their absolute values. [b] Derived errors in parentheses in units of the last digit. These were calculated according to Constain's formula: $\sigma(x) = K/|x|$; $\sigma(x)$ is the error in the coordinate $\times$ and K = 0.0012 Å. [c] Imaginary number obtained and the value is constrained to zero.

Table 6
Comparison between substitution and equilibrium MP2/6–311++G(d,p) coordinates determined for the hydrogen atoms of the water subunit in the *ap* – *m* complex.

	MVK···**H**OH[a]		MVK···HO**H**[b]	
	r_s	r_e	r_s	r_e
|*a*|[c]	2.29166(69)[d]	2.408	3.84105(41)[d]	3.903
|*b*|	0.4052(39)	0.415	0.4295(37)	0.403
|*c*|	0[e]	0.021	0.154(10)	0.249

[a] These coordinates are those for the bonded H atom of the water subunit. [b] These coordinates are those for the non – bonded H atom of the water subunit. [c] *a*, *b* and *c* are the coordinates in angstroms in their absolute values. [d] Derived errors in parentheses in units of the last digit. These were calculated according to Constain's formula: $\sigma(x) = K/|x|$; $\sigma(x)$ is the error in the coordinate $\times$ and K = 0.0012 Å. [e]Imaginary number obtained and the value is constrained to zero.

Table 7
Intermolecular HB parameters derived from the partial r_0 geometry of the *ap* – *m* complex. Bond distances in Å and angles in degrees.

	Experimental	Calculated[c]
r (H_w···O_{mvk})[a]	1.9669(99)[b]	1.95
r (O_w ···H_{mvk})	2.436(64)	2.51
∠ (O_w – H_w···O_{mvk})	163.39(87)	162.5
τ (H_w – O_w – H_w···O_{mvk})	133.4(47)	162.4

[a] The subindexes *w* or *mvk* indicate that the atom belongs to the water or MVK moieties, respectively (see Fig. 3). [b] Errors in parentheses in units of the last digit. [c] MP2/6–311++G(d,p) level of theory

were also determined from our analysis. While δ could be fitted for all the isomers, ε was only determined for the *sp* – *m* isomer. The F_0 value, which is associated with the moment of inertia of the methyl top, could not be determined in the present fits, so it was fixed to the values derived from the *ab initio* geometries. The experimental values for V_3 barrier heights for *ap* – *m*, *ap* – *v*, *sp* – *m* and *sp* – *v* are 389.80(43), 418.5(17), 349.59(26) and 359.99(34) cm^{-1}, respectively. These values are slightly lower than those determined before for the MVK monomers [24]. The V_3 values for *ap* – MVK and *sp* – MVK monomers are 443.236(78) and 385.28(30) cm^{-1}, respectively. Both *ap* – *m* and *sp* – *m* isomers have an intermolecular interaction between the oxygen atom of water and one hydrogen of the methyl top, which should raise the V_3 barrier. Surprisingly, the declining trend of V_3 values is the same for the four isomers. This behaviour has been already found by Lei *et al.* [39] in a related molecular system like the monohydrate of acetophenone. The authors justified the V_3 decrease from 627.0(25) to 588.5(42) cm^{-1}, acetophenone and acetophenone – H_2O, respectively, as an electron density depletion at the oxygen of water. Using an NBO analysis, they observed a limited charge transfer flowing from hydrogen in H_2O to the oxygen atom, which, indeed, increases its negative charge. The argument given by Lei *et al.* can be applied to explain the V_3 decreasing for the four MVK – H_2O isomers. Additionally, there is another obvious reasoning to explain the smaller V_3 values when passing from the monomer to the water complex. As shown by Apponi *et al.* [40], the reduction of the V_3 when passing from acetone to hydroxyacetone is mainly due to the internal hydrogen bond between the carbonyl oxygen and hydroxyl hydrogen that removes electron density from the carbonyl oxygen. This reasoning was used by Ouyang & Howard to justify the V_3 decreasing in the monohydrate of acetic acid [41]. Several examples are also reported by Fabero *et al.* in the study of the molecular adduct 1,1,1-trifluoroacetone – water, which show the change in the V_3 barrier of the internal rotation of the methyl group upon interaction with water [42].

Interestingly, the experimental values for V_3 barrier heights for "*m*" complexes are slightly smaller than those for the "*v*" complexes. It would be expected that the C – H···O secondary interaction between the methyl group and the oxygen of the water molecule in "*m*" complexes increases the V_3 barrier (or hinder the internal rotation of the methyl group), but the effect is completely the opposite. The same behaviour has been observed for the water complex of the *syn* – conformer of the Criegee intermediate CH_3CHOO [43]. The V_3 value for *syn* – CH_3CHOO – H_2O complex was found to be 699.3(32) cm^{-1}, much lower than the V_3 value reported for the *syn* – CH_3CHOO conformer, 837.1(17) cm^{-1}. Cabezas & Endo [43] rationalized this decrease by taking into account the HB interactions established within the *syn* – CH_3CHOO monomer, the *syn* – CH_3CHOO – H_2O and their corresponding internal rotation transition state. They found that the partial stabilization induced by water HBs is larger in the transition state of the *syn* – CH_3CHOO – H_2O complex than at the minimum and consequently the V_3 barrier is lower than in the case of the monomer. As shown in Fig. 4, for the *ap* – *m* complex, the water oxygen interacts with one methyl hydrogen at the minimum, while for TS–*ap* – *m*, the rotated position of the methyl group allows the establishment of two bifurcated HBs between the water oxygen and two methyl hydrogens. This also occurs in the internal rotation TS of the *sp* – *m* complex, while does not occur in any of the "*v*" complexes. Hence, this partial stabilization induced by water HBs slightly reduces the energy of the TS in the case of the "*m*" complexes compared to that of the "*v*" complexes and consequently the V_3 barrier is lower in the former complexes.

5. Conclusions

In the present study, the rotational spectra of the 1:1 adducts of MVK with water and their isotopologues have been investigated using chirped – pulse and cavity – based FTMW spectroscopy. Four different isomers have been observed and characterized for the first time. The most abundant species prefer the *ap* conforma-

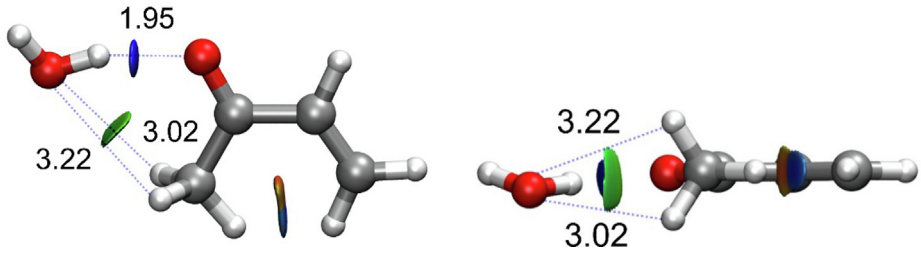

Fig. 4. Different perspectives of the MP2/6–311++G(d,p) structure of the methyl internal rotation transition state of the *ap* − *m* isomer showing their NCI isosurfaces (*s* = 0.5). Intermolecular HBs are indicated with dashed lines and the bond lengths are given in Å.

tion of the MVK subunit and are stabilized by a network of two intermolecular O − H···O and C − H···O interactions. As in bare MVK, all the complexes show *A* − *E* spectral splitting arising from the internal rotation of the methyl group. Our results deepen the possible interactions of MVK in the atmosphere and illustrate the ability of water to interact with MVK. Follow − up studies of MVK − H_2O isomer specific reactivity may be important to improve the predictive power of atmospheric chemistry models.

CRediT authorship contribution statement

Carlos Cabezas: Conceptualization, Methodology, Investigation, Formal analysis, Data curation, Writing – original draft. **Marcos Juanes:** Investigation, Formal analysis, Writing – review & editing. **Rizalina T. Saragi:** Investigation, Formal analysis, Writing – review & editing. **Alberto Lesarri:** Methodology, Resources, Writing – review & editing. **Isabel Peña:** Methodology, Formal analysis, Investigation, Data curation, Writing – original draft.

Declaration of Competing Interest

The authors declare that they have no known competing financial interests or personal relationships that could have appeared to influence the work reported in this paper.

Acknowledgments

This research was funded by the Spanish Ministerio de Ciencia e Innovación (PID2020-117925GA-I00 and PGC2018-098561-B-C22). M. J. and R. T. S. thank predoctoral contracts from the MICINN and UVa, respectively. The authors would like to thank Jesús María Martínez de Ilarduya for providing the MVK sample and Laura Galindo Ciprián for helping with frequency and intensity measurements.

Appendix A. Supplementary data

Supplementary data to this article can be found online at https://doi.org/10.1016/j.saa.2021.120846.

References

[1] J. Zhu, J.E. Penner, G. Lin, C. Zhou, L.i. Xu, B. Zhuang, Mechanism of SOA formation determines magnitude of radiative effects, Proc. Natl. Acad. Sci. U. S. A. 114 (48) (2017) 12685–12690, https://doi.org/10.1073/pnas.1712273114.

[2] M. Ehn, J.A. Thornton, E. Kleist, M. Sipilä, H. Junninen, I. Pullinen, M. Springer, F. Rubach, R. Tillmann, B. Lee, F. Lopez-Hilfiker, S. Andres, I.-H. Acir, M. Rissanen, T. Jokinen, S. Schobesberger, J. Kangasluoma, J. Kontkanen, T. Nieminen, T. Kurtén, L.B. Nielsen, S. Jørgensen, H.G. Kjaergaard, M. Canagaratna, M.D. Maso, T. Berndt, T. Petäjä, A. Wahner, V.-M. Kerminen, M. Kulmala, D.R. Worsnop, J. Wildt, T.F. Mentel, A large source of low-volatility secondary organic aerosol, Nature 506 (7489) (2014) 476–479, https://doi.org/10.1038/nature13032.

[3] F. Riccobono, S. Schobesberger, C.E. Scott, J. Dommen, I.K. Ortega, L. Rondo, J. Almeida, A. Amorim, F. Bianchi, M. Breitenlechner, A. David, A. Downard, E.M. Dunne, J. Duplissy, S. Ehrhart, R.C. Flagan, A. Franchin, A. Hansel, H. Junninen, M. Kajos, H. Keskinen, A. Kupc, A. Kürten, A.N. Kvashin, A. Laaksonen, K. Lehtipalo, V. Makhmutov, S. Mathot, T. Nieminen, A. Onnela, T. Petäjä, A.P. Praplan, F.D. Santos, S. Schallhart, J.H. Seinfeld, M. Sipilä, D.V. Spracklen, Y. Stozhkov, F. Stratmann, A. Tomé, G. Tsagkogeorgas, P. Vaattovaara, Y. Viisanen, A. Vrtala, P.E. Wagner, E. Weingartner, H. Wex, D. Wimmer, K.S. Carslaw, J. Curtius, N.M. Donahue, J. Kirkby, M. Kulmala, D.R. Worsnop, U. Baltensperger, Oxidation products of biogenic emissions contribute to nucleation of atmospheric particles, Science 344 (6185) (2014) 717–721.

[4] K. Cheung, H. Guo, J.M. Ou, I.J. Simpson, B. Barletta, S. Meinardi, D.R. Blake, Diurnal profiles of isoprene, methacrolein and methyl vinyl ketone at an urban site in Hong Kong, Atmos. Environ. 84 (2014) 323–331, https://doi.org/10.1016/j.atmosenv.2013.11.056.

[5] S.S. Brown, J.A. Degouw, C. Warneke, T.B. Ryerson, W.P. Dubé, E. Atlas, R.J. Weber, R.E. Peltier, J.A. Neuman, J.M. Roberts, A. Swanson, F. Flocke, S.A. McKeen, J. Brioude, R. Sommariva, M. Trainer, F.C. Fehsenfeld, A.R. Ravishankara, Nocturnal isoprene oxidation over the Northeast United States in summer and its impact on reactive nitrogen partitioning and secondary organic aerosol, Atmos. Chem. Phys. 9 (2009) 3027–3042, https://doi.org/10.5194/acp-9-3027-2009.

[6] T.A. Biesenthal, Q. Wu, P.B. Shepson, H.A. Wiebe, K.G. Anlauf, G.I. Mackay, A study of relationships between isoprene, its oxidation products, and ozone, in the Lower Fraser Valley, BC, Atmos. Environ. 31 (14) (1997) 2049–2058, https://doi.org/10.1016/S1352-2310(96)00318-4.

[7] S.N. Matsunaga, C. Wiedinmyer, A.B. Guenther, J.J. Orlando, T. Karl, D.W. Toohey, J.P. Greenberg, Y. Kajii, Isoprene oxidation products are a significant atmospheric aerosol component, Atmos. Chem. Phys. Discuss. 5 (2005) 11143–11156.

[8] V. Vaida, Perspective: Water cluster mediated atmospheric chemistry, J. Chem. Phys. 135 (2011) 1–8, https://doi.org/10.1063/1.3608919.

[9] B. Ervens, P. Renard, S. Tlili, S. Ravier, J. Clement, A. Monod, Aqueous-phase oligomerization of methyl vinyl ketone through photooxidation - Part 2: Development of the chemical mechanism and atmospheric implications To cite this version : HAL Id : hal-01436851 Aqueous-phase oligomerization of methyl vinyl ketone thr, Atmos. Chem. Phys. 15 (2015) 9109–9127, https://doi.org/10.5194/acp-15-9109-2015.

[10] T.B. Nguyen, P.J. Roach, J. Laskin, A. Laskin, S.A. Nizkorodov, Effect of humidity on the composition of isoprene photooxidation secondary organic aerosol, Atmos. Chem. Phys. 11 (14) (2011) 6931–6944, https://doi.org/10.5194/acp-11-6931-201110.5194/acp-11-6931-2011-supplement.

[11] B.K. Pun, C. Seigneur, Investigative modeling of new pathways for secondary organic aerosol formation, Atmos. Chem. Phys. 7 (2007) 2199–2216, https://doi.org/10.5194/acp-7-2199-2007.

[12] J.H. Seinfeld, G.B. Erdakos, W.E. Asher, J.F. Pankow, Modeling the formation of secondary organic aerosol (SOA). 2. The predicted effects of relative humidity on aerosol formation in the α-pinene-, β-pinene-, sabinene-, Δ3-carene-, and cyclohexene-ozone systems, Environ. Sci. Technol. 35 (2001) 1806–1817, https://doi.org/10.1021/es001765+.

[13] E.G. Schnitzler, C. Badran, W. Jäger, Contrasting effects of water on the barriers to decarboxylation of two oxalic acid monohydrates: a combined rotational spectroscopic and ab initio study, J. Phys. Chem. Lett. 7 (7) (2016) 1143–1147, https://doi.org/10.1021/acs.jpclett.6b0027810.1021/acs.jpclett.6b00278.s001.

[14] Y. Sakamoto, R. Yajima, S. Inomata, J. Hirokawa, Water vapour effects on secondary organic aerosol formation in isoprene ozonolysis, Phys. Chem. Chem. Phys. 19 (4) (2017) 3165–3175.

[15] S.I. Murugachandran, J. Tang, I. Peña, D. Loru, M.E. Sanz, New Insights into Secondary Organic Aerosol Formation: Water Binding to Limonene, J. Phys. Chem. Lett. 12 (3) (2021) 1081–1086, https://doi.org/10.1021/acs.jpclett.0c0357410.1021/acs.jpclett.0c03574.s001.

[16] M. Chrayteh, T.R. Huet, P. Dréan, Microsolvation of myrtenal studied by microwave spectroscopy highlights the role of quasi-hydrogen bonds in the stabilization of its hydrates, J. Chem. Phys. 153 (10) (2020) 104304, https://doi.org/10.1063/5.0019957.

[17] M. Chrayteh, A. Savoia, T.R. Huet, P. Dréan, Microhydration of verbenone: How the chain of water molecules adapts its structure to the host molecule, Phys. Chem. Chem. Phys. 22 (10) (2020) 5855–5864.

[18] C. Pérez, A. Krin, A.L. Steber, J.C. López, Z. Kisiel, M. Schnell, Wetting Camphor: Multi-Isotopic Substitution Identifies the Complementary Roles of Hydrogen

Bonding and Dispersive Forces, J. Phys. Chem. Lett. 7 (1) (2016) 154–160, https://doi.org/10.1021/acs.jpclett.5b0254110.1021/acs.jpclett.5b02541.s001.
[19] E.M. Neeman, J.R. Avilés Moreno, T.R. Huet, Gas-phase hydration of nopinone: the interplay between theoretical methods and experiments unveils the conformational landscape, Phys. Chem. Chem. Phys. 23 (33) (2021) 18137–18144.
[20] S. Blanco, J.C. López, A. Maris, Terpenoids: Shape and non-covalent interactions. The rotational spectrum of: Cis -verbenol and its 1 : 1 water complex, Phys. Chem. Chem. Phys. 22 (2020) 5729–5734. DOI: 10.1039/d0cp00086h.
[21] M. Chrayteh, E. Burevschi, D. Loru, T.R. Huet, P. Dréan, M.E. Sanz, Disentangling the complex network of non-covalent interactions in fenchone hydrates via rotational spectroscopy and quantum chemistry, Phys. Chem. Chem. Phys. 23 (36) (2021) 20686–20694.
[22] P.D. Foster, V.M. Rao, R.F. Curl, Microwave spectrum of methyl vinyl ketone, J. Chem. Phys. 43 (3) (1965) 1064–1066.
[23] D.S. Wilcox, A.J. Shirar, O.L. Williams, B.C. Dian, Additional conformer observed in the microwave spectrum of methyl vinyl ketone, Chem. Phys. Lett. 508 (1-3) (2011) 10–16, https://doi.org/10.1016/j.cplett.2011.04.001.
[24] O. Zakharenko, R.A. Motiyenko, J.R. Aviles Moreno, T.R. Huet, Conformational landscape and torsion-rotation-vibration effects in the two conformers of methyl vinyl ketone, a major oxidation product of isoprene, J. Phys. Chem. A. 121 (34) (2017) 6420–6428, https://doi.org/10.1021/acs.jpca.7b0636010.1021/acs.jpca.7b06360.s001.
[25] C. Møller, M.S. Plesset, Note on an approximation treatment for many-electron systems, Phys. Rev. 46 (1934) 618–622, https://doi.org/10.1093/ejcts/ezx458.
[26] M.J. Frisch, J.A. Pople, J.S. Binkley, Self-consistent molecular orbital methods 25. Supplementary functions for Gaussian basis sets, J. Chem. Phys. 80 (7) (1984) 3265–3269, https://doi.org/10.1063/1.447079.
[27] M.J. Frisch, G.W. Trucks, H.B. Schlegel, G.E. Scuseria, M.A. Robb, J.R. Cheeseman, G. Scalmani, V. Barone, G.A. Petersson, H. Nakatsuji, X. Li, M. Caricato, A.V. Marenich, J. Bloino, B.G. Janesko, R. Gomperts, B. Mennucci, H.P. Hratchian, J.V. Ortiz, A.F. Izmaylov, J.L. Sonnenberg, D. Williams-Young, F. Ding, F. Lipparini, F. Egidi, J. Goings, B. Peng, A. Petrone, T. Henderson, D. Ranasinghe, V.G. Zakrzewski, J. Gao, N. Rega, G. Zheng, W. Liang, M. Hada, M. Ehara, K. Toyota, R. Fukuda, J. Hasegawa, M. Ishida, T. Nakajima, Y. Honda, O. Kitao, H. Nakai, T. Vreven, K. Throssell, J.A. Montgomery Jr., J.E. Peralta, F. Ogliaro, M.J. Bearpark, J.J. Heyd, E.N. Brothers, K.N. Kudin, V.N. Staroverov, T.A. Keith, R. Kobayashi, J. Normand, K. Raghavachari, A.P. Rendell, J.C. Burant, S.S. Iyengar, J. Tomasi, M. Cossi, J.M. Millam, M. Klene, C. Adamo, R. Cammi, J.W. Ochterski, R. L. Martin, K. Morokuma, O. Farkas, J.B. Foresman, D.J. Fox, Gaussian~16 Revision C.01 (2016).
[28] M. Juanes, W. Li, L. Spada, L. Evangelisti, A. Lesarri, W. Caminati, Internal dynamics of cyclohexanol and the cyclohexanol-water adduct, Phys. Chem. Chem. Phys. 21 (7) (2019) 3676–3682.
[29] J.-U. Grabow, W. Stahl, H. Dreizler, A multioctave coaxially oriented beam-resonator arrangement Fourier-transform microwave spectrometer, Rev. Sci. Instrum. 67 (12) (1996) 4072–4084, https://doi.org/10.1063/1.1147553.
[30] T.J. Balle, W.H. Flygare, Fabry-Pérot cavity pulsed Fourier transform microwave spectrometer with a pulsed nozzle particle source, Rev. Sci. Instrum. 52 (1981) 33–45, https://doi.org/10.1063/1.1136443.
[31] J. Demaison, N. Vogt, Y. Jin, R.T. Saragi, M. Juanes, A. Lesarri, How accurate is the determination of equilibrium structures for van der Waals complexes? The dimer $N_2O\cdots CO$ as an example, J. Chem. Phys. 154 (19) (2021) 194302, https://doi.org/10.1063/5.0048603.
[32] H. Hartwig, H. Dreizler, The microwave spectrum of trans-2,3-dimethyloxirane in torsional excited states, Zeitschrift Für Naturforsch A 51 (1996) 923–932, https://doi.org/10.1515/zna-1996-0807.
[33] J.K.G. Watson, Determination of centrifugal distortion coefficients of asymmetric-top molecules, J. Chem. Phys. 46 (5) (1967) 1935–1949, https://doi.org/10.1063/1.1840957.
[34] R.C. Woods, A general program for the calculation of internal rotation splittings in microwave spectroscopy, J. Mol. Spectrosc. 21 (1-4) (1966) 4–24, https://doi.org/10.1016/0022-2852(66)90117-2.
[35] J. Contreras-García, E.R. Johnson, S. Keinan, R. Chaudret, J.-P. Piquemal, D.N. Beratan, W. Yang, NCIPLOT: A program for plotting noncovalent interaction regions, J. Chem. Theory Comput. 7 (3) (2011) 625–632, https://doi.org/10.1021/ct100641a.
[36] L. Evangelisti, W. Caminati, Internal dynamics in complexes of water with organic molecules. Details of the internal motions in tert-butylalcohol–water, Internal dynamics in complexes of water with organic molecules. Details of the internal motions in tert -butylalcohol – water 12 (43) (2010) 14433, https://doi.org/10.1039/c0cp01195a.
[37] J. Kraitchman, Determination of molecular structure from microwave spectroscopic data, Am. J. Phys. 21 (1) (1953) 17–24, https://doi.org/10.1119/1.1933338.
[38] Z. Kisiel, PROSPE-Programs for Rotational spectroscopy, Spectrosc. from Sp. (2001) 91–106, https://doi.org/10.1007/978-94-010-0832-7_6.
[39] J. Lei, J. Zhang, G. Feng, J.-U. Grabow, Q. Gou, Conformational preference determined by inequivalent n-pairs: rotational studies on acetophenone and its monohydrate, Phys. Chem. Chem. Phys. 21 (41) (2019) 22888–22894, https://doi.org/10.1039/C9CP03904J.
[40] A.J. Apponi, J.J. Hoy, D.T. Halfen, L.M. Ziurys, M.A. Brewster, Hydroxyacetone (CH_3COCH_2OH): A combined microwave and millimeter-wave laboratory study and associated astronomical search, Astrophys. J. 652 (2) (2006) 1787–1795, https://doi.org/10.1086/508157.
[41] B. Ouyang, B.J. Howard, The monohydrate and dihydrate of acetic acid: A high-resolution microwave spectroscopic study, Phys. Chem. Chem. Phys. 11 (2) (2009) 366–373, https://doi.org/10.1039/B814562H.
[42] L.B. Favero, L. Evangelisti, A. Maris, A. Vega-Toribio, A. Lesarri, W. Caminati, How trifluoroacetone interacts with water, J. Phys. Chem. A. 115 (34) (2011) 9493–9497, https://doi.org/10.1021/jp112015r.
[43] C. Cabezas, Y. Endo, The reactivity of the Criegee intermediate CH_3CHOO with water probed by FTMW spectroscopy, J. Chem. Phys. 148 (1) (2018) 014308, https://doi.org/10.1063/1.5009033.